Synthetic-Aperture Silhouette Imaging (SASI): Laboratory Demonstration Traceable to Ground-Based Imaging of GEO Satellites

Richard G. Paxman*, Kurt W. Gleichman, Alexander S. Iacchetta, and Bradley M. Jost
Maxar Technologies Inc., 1200 Joe Hall Drive, Ypsilanti, MI 48197
** rick.paxman@maxar.com*

ABSTRACT

Synthetic-Aperture Silhouette Imaging (SASI) is a cost-effective approach for ground-based imaging of silhouettes of geosynchronous satellites at fine resolution. Such fine-resolution silhouettes are very informative. They enable estimates of satellite pose, provide diagnostic information about the deployment of antennas and solar panels, and reveal the presence and geometry of nearby satellites in rendezvous and proximity operations. We report on a laboratory demonstration of SASI that is a scaled version of the ground-based geosynchronous-satellite imaging geometry. The resolution achieved is equivalent to that of a 60m diameter telescope with adaptive optics.

1. SASI CONCEPT

The problem of ground-based fine-resolution imaging of Geosynchronous Earth Orbit (GEO) satellites continues to be an important unsolved space-surveillance problem. If one wants to achieve 10cm resolution at a range of 36,000km (range to a geosynchronous satellite) at a wavelength of 0.5μm via conventional means, then a 180m diameter telescope with adaptive optics is needed. Such a system is prohibitively expensive and is currently not within technical reach. This capability gap has led researchers to investigate interferometric-imaging approaches in which the baselines are sufficiently large (e.g. 180m) to collect the spatial-frequency information needed to achieve the desired resolution on target. We are investigating a passive-illumination approach which is radically different from amplitude, intensity, or heterodyne-interferometry approaches. This approach, called SASI, produces a fine-resolution image of the satellite silhouette.

When plane-wave radiation emanating from a bright star is occluded by a geosynchronous satellite, the light is diffracted and a moving diffraction pattern (or shadow) is cast on the surface of the earth, as illustrated in Fig. 1.

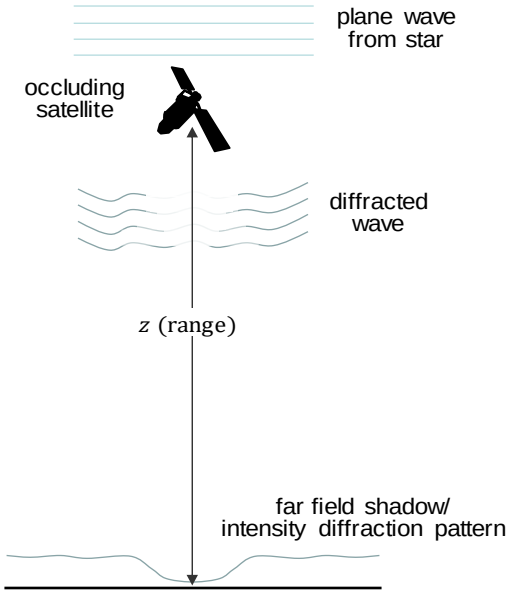

Fig. 1. A moving diffraction pattern (shadow) is created when starlight is diffracted by an occluding satellite.

With prior knowledge of the satellite orbit and star location, the track of the moving shadow, which moves from west to east, can be predicted. A north-south linear array of inexpensive hobby telescopes can be deployed roughly perpendicular to the west-to-east shadow track to collect a time history of the star intensity as the shadow passes by. This synthetic aperture allows us to capture the entire 2D intensity diffraction pattern cast by the occluding satellite, as illustrated in Fig. 2. Given the Fresnel diffraction pattern and use of the constraint that the object is binary (a silhouette), we can use phase-retrieval techniques to obtain a fine-resolution image of the silhouette.

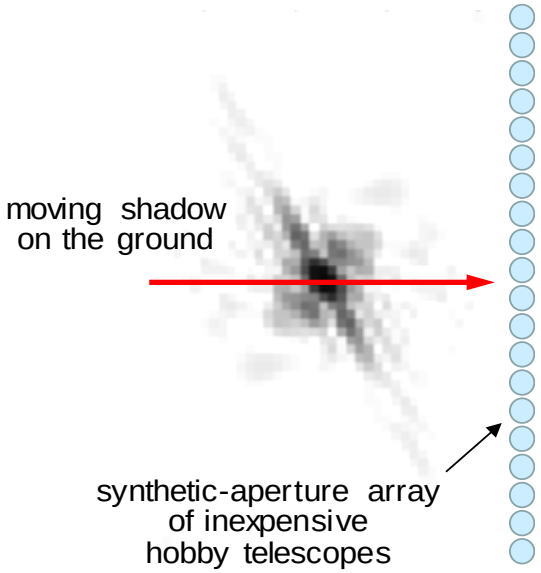

Fig. 2. A west-to-east moving intensity diffraction pattern can be captured with temporal synthesis using a linear array of inexpensive hobby telescopes.

A compelling reason to pursue the SASI concept is that it is extremely cost effective relative to other ground-based approaches. The hardware required is embarrassingly inexpensive. SASI only requires an array of tracking hobby-class telescopes, each with a low-cost APD detector. The telescopes can be deployed in a linear array that spans the desired effective diameter. Each telescope tracks the designated star and collects its time history of the detected light with the aid of a field stop and a single APD detector. Signals must be detected at ~10kHz sampling rates and must be synchronized to sub-millisecond accuracy, which is straightforward to achieve. The linear array with temporal samples allows us to reconstitute a 2D data set via temporal synthesis. The telescope/sensor modules can be identical, enabling economies of scale.

Another advantage of the SASI concept is that the signal depends on the star magnitude, not the magnitude of the satellite. The target satellite can be arbitrarily faint. In fact, SASI works well for unilluminated satellites (in the earth's shadow) or satellites with low optical signature. Countermeasures against imaging based on occlusion are very difficult to engineer. SASI is also insensitive to atmospheric-turbulence effects, unlike many ground-based observational methods. SASI indirectly measures Fresnel amplitude, which is insensitive to turbulence-induced aberrations, so long as the turbulence is near the pupil. This obviates the need for phase-tracking and wavefront-sensing instrumentation.

Fine-resolution silhouettes differ from conventional gray-scale images, but they are very informative. Silhouettes enable estimates of satellite pose, provide diagnostic information about deployment of antennas and solar panels, and reveal the presence of nearby satellites in rendezvous and proximity operations. Silhouettes also complement gray-level images, providing information about regions not illuminated as well as providing a valuable support constraint for use with interferometric-imaging data. SASI data can also help refine orbital parameters.

The use of SASI for imaging satellites, also referred to as shadow imaging, was first proposed by Burns [1] and has been studied by others [2-9]. We formulated the SASI concept without knowledge of other's work, which gave us an independent perspective. Our contribution involves developing a novel algorithm and demonstrating the SASI concept in the laboratory.

2. ALGORITHM

SASI data consist of time-series values for each telescope in a linear array. We use temporal synthesis to form a 2D spatial intensity diffraction pattern that bears little resemblance to a silhouette. An algorithm is used to produce a literal silhouette from these non-literal data. Such an algorithm can be interpreted as a phase-retrieval algorithm. Since we have an indirect measurement of the amplitude (square root of the measured intensity) of the complex field at the ground, if we were able to retrieve the phase, we could then back propagate to get the complex field in the target plane. The complex field in the target plane will have uniform phase and an amplitude that is the satellite silhouette. Phase-retrieval algorithms rely on prior knowledge. We refer to the prior knowledge utilized for SASI, namely uniform phase and binary amplitude in the target plane, as an opacity constraint. Opacity has been shown to be a powerful constraint in other settings [10-12].

Our algorithm is based on nonlinear optimization of an estimate of the silhouette from data. Simulated light, diffracted by an estimated silhouette, is propagated to the plane of the data through a Fresnel transform. Employing Babinet's principal allows the discrete Fresnel propagation to be well behaved provided the silhouette is properly sampled. Since diffraction is wavelength dependent, we perform the propagation at 11 sample wavelengths to model the spectral bandwidth (630-670 nm) of the SASI sensor. The net diffraction pattern is the incoherent sum of the individual wavelength-dependent diffraction patterns. The resulting net diffraction pattern is then appropriately sampled according to the aperture size and spacing used to collect the data. A data-consistency metric is then computed for the estimated silhouette. This metric can be minimized through nonlinear optimization of the silhouette parameters. The silhouette is subject to constraints that prevent values less than zero or greater than one. Regularization terms or silhouette parameterization are used to force values to be close to zero or one, similar to techniques employed when recovering amplitude in other phase-retrieval problems [13]. Nonlinear optimization allows other nuisance terms to be estimated in addition to the silhouette. For example, the distance from the silhouette plane to the data plane can be refined through the optimization process. The position of the subapertures used to collect the data can also be refined.

3. EXPERIMENTAL DESIGN

Multiple researchers have demonstrated SASI (shadow imaging) in simulation. To test the SASI concept with real data, we designed a scaled laboratory experiment that directly traces to the geosynchronous-satellite imaging geometry. The GEO-satellite-to-laboratory scaling is governed by the Fresnel-diffraction integral equation [14],

$$U(x_o, y_o) = \frac{e^{jkz}}{j\lambda z} \iint_{-\infty}^{\infty} U(x_1, y_1) exp\left\{ j \frac{k}{2z} [(x_o - x_1)^2 + (y_o - y_1)^2] \right\} dx_1 dy_1 \,, \quad (1)$$

where $U(x_o, y_o)$ is the complex scaler field at the ground, j is the unit imaginary number, λ is the wavelength, $k = 2\pi/\lambda$, z is the range from the satellite to the ground, and $U(x_1, y_1)$ is the complex field in the target plane, immediately after occlusion by the satellite. Careful inspection of Equation (1) reveals that applying a demagnification factor in the transverse direction, i.e. in the plane of the receiver (x_o, y_o) and satellite (x_1, y_1), while holding the wavelength constant, requires the scaling factor to be squared in the range dimension, z. Fortuitously, in scaling from the Geo satellite geometry to the laboratory, the resulting dimensions are readily accommodated on a standard optical bench, as summarized in Table 1.

Table 1. Summary of mapping from Geo-Satellite to Laboratory Scale

Parameter	GEO-Satellite Value	Laboratory Value
Distance from receiver array to satellite	36,000 km	0.36 m
Length of receiver array	200 m	0.02 m
Circumscribing diameter of satellite	10 m	0.001 m

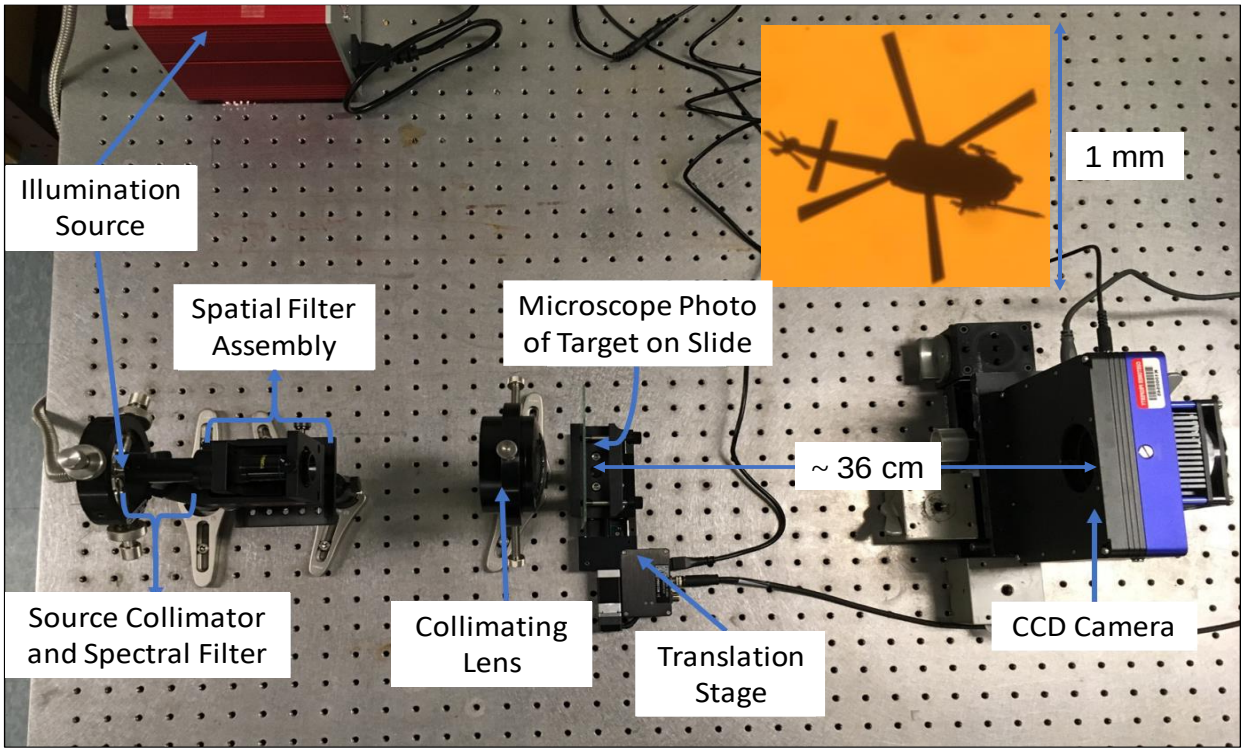

Fig. 3. Layout of SASI laboratory experiment. The inset is a microscope photograph of the binary target.

The experimental setup is shown in Fig.3. The star simulator uses a high-intensity fiber-bundle-coupled illuminator with a 150-W Halogen bulb at a color temperature of 3200K. The output of the 6.4-mm fiber bundle is focused into a pinhole via a microscope objective. We used a 2µm pinhole and a 40nm spectral filter centered at 650nm. The output of the pinhole is collimated with a 150-mm F/2 lens. The pinhole size was selected as a compromise between emulating a star diameter and having enough light so that the exposure time is not too long. The 2µm pinhole produced diffraction fringes with contrast that visually matches our simulations, even though the effective angular star diameter is 2.75 arcseconds, far larger than even the largest angular diameter among stars in the night sky.

The collimated light, emulating light from a distant star, illuminates a microscope slide on which an opaque helicopter silhouette was fabricated. The chrome-deposition process was performed for us by Applied Image, Inc. The on-slide resolution achieved by this process is 2.5µm. A microscope photograph of the occluding target is shown as an inset in the figure. The extent (circumscribing diameter) of the on-slide helicopter silhouette is 1mm which corresponds to a 10m target in a geosynchronous orbit. The diffracted light travels to the detector array. A deployed SASI system consists of a linear array of telescopes with an orientation orthogonal to the direction of shadow movement. For the laboratory, we used a focal-plane camera, which allows for flexibility in emulating a variety of array configurations. The camera we used was a QHY 16200A monochrome astronomical camera with 6µm square pixels and a format of 4656 x 3522 pixels. This camera has low read noise (10 electrons), low dark current (0.04 electrons/pixel/s), relatively high quantum efficiency (50%), and flexibility on integration time (1ms to 10,000 seconds). The laboratory demonstration of SASI emulates the linear telescope array by using a linear array of non-adjacent binned pixels, approximating the telescope's aperture and spacing in a deployed system. To emulate the light-bucket collection by hobby telescopes, we binned the signal in 5-pixel diameter regions on the camera with laboratory dimensions of 30µm, effectively simulating 30cm apertures in a deployed telescope array.

Because the focal-plane array allows the entire 2D intensity diffraction pattern to be collected without movement of the star, and at finer sampling than the fielded system, data from the laboratory has utility for design trades and algorithm development supporting the design of a fielded SASI system. We had initially planned to emulate temporal synthesis by translating the object slide linearly, but we determined that the linear motion of the stage would not provide more insight into the shadow's motion observed with a deployed telescope array. The linear motion of the stage would ultimately introduce non-realistic errors into the experimental measurements, in part due to the long

integration times required to obtain adequate signal. We believe that simulation of the apertures is sufficiently representative of the data collected by a telescope array. We had also intended to insert a phase screen proximate to the focal plane to emulate atmospheric turbulence. However, the extent of atmospheric turbulence is such a small fraction of the range to a geosynchronous orbit that the corresponding scaled laboratory design would require this phase screen to be 10μm from the detector array. Of course, we don't have a phase screen that is this thin, so instead we rely on simulation to demonstrate the immunity of SASI to atmospheric turbulence.

4. RESULTS

When taking our first measurements, we discovered that dust and imperfections in the illumination system degrade the quality of our measurements. To mitigate this issue, we implemented calibration measurements that allow us to perform both bias subtraction and flat-fielding of our science measurements. The in-laboratory detected Fresnel intensity diffraction pattern is shown in Fig. 4. To get this intensity data, we aggregated pixels on our camera to emulate a linear array of 30cm diameter hobby telescopes placed 60cm apart (50% duty cycle). The collected data closely match simulated data derived by computing the Fresnel diffraction pattern from our target model. The only noticeable difference is that the laboratory data has a low level of mottled texture which we attribute to the optical quality of the slide surfaces. Upon investigation of those aberrations we discovered that the phase errors just after the glass slide have a peak-to-valley on the order of about 10 nm, which is well within the specification of wavefront error for even very well-polished optical surfaces. These phase errors and the associated mottled texture are artificial and would not appear in data from a fielded system, since there is no microscope slide in space. Despite the errors introduced by the unrealistic phase aberrations, we are still able to reconstruct the target's silhouette by employing regularization techniques.

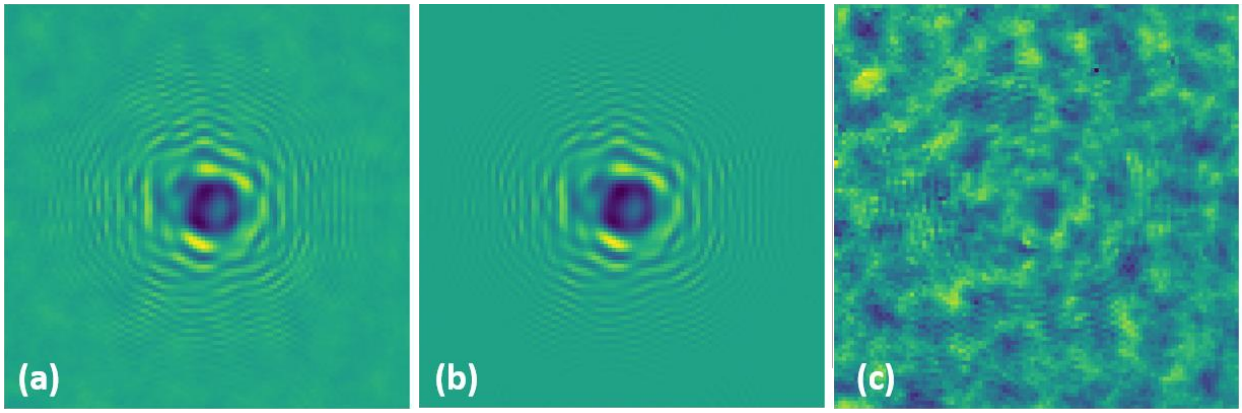

Fig. 4. SASI laboratory data compares favorably with simulated data. (a) The laboratory intensity diffraction pattern formed by diffraction of emulated starlight by an opaque helicopter silhouette. The color scale has navy as the darkest value, yellow as the brightest value, and the green in the periphery is the signal in the absence of a diffracting satellite. (b) Modelled (expected) data. (c) The difference image between (a) and (b), scaled to utilize the full dynamic range, is believed to be due to microscope-slide-induced phase aberrations.

As expected, the diffraction pattern is non-literal, and it would be difficult for an analyst to infer the shape of the occluding target by examining the raw data. The diffraction pattern is seen to be dark (a shadow) in the center surrounded by chirp-like fringes whose period reduces with distance from the center. The value in the extreme periphery is the level of light that is observed from the star in the absence of an occluder. In addition to creating shadow depressions, diffraction creates features that are brighter than the unoccluded baseline value. In both the laboratory data and the modelled data, we can see evidence of undersampling artifact when the fringes become closely spaced. This artifact would be reduced or eliminated if we used finer spatial sampling with the equivalent telescope array. The sources of systematic error, listed in order on impact to image restoration, are mottled texture arising from slide-induced aberrations, pinhole extent (equivalent star diameter), and undersampling.

We performed an analysis of the laboratory data in the absence of an occluding satellite, considering photon and read noise, and found the electric-voltage SNR to be 684. We were able to find the equivalent star magnitude that would give the comparable SNR with field data. This analysis requires knowing the hobby-telescope diameter, the speed of the shadow track on the ground, the temporal sampling, and the optical bandwidth. The equivalent star magnitude turns out to be a very bright visual magnitude, $M_v = 0.4$. There are only a handful of stars in the night sky brighter than this. Our intent in collecting high-SNR data was to facilitate identification of systematic errors without them being masked by noise. These laboratory results anchor our simulations in the limiting case of high-SNR data. Performance as a function of star magnitude has been explored extensively in simulation [3], where Douglas reports retrieving informative silhouette estimates with $M_v = 10$ stars for varying system designs and target sizes.

We estimated the object by iteratively optimizing an objective function that penalizes deviations from a binary object and discrepancies from the laboratory data. The resulting estimate is shown in Fig. 5 along with the true object. Clearly the estimated image is a high-fidelity representation of the truth and has significant intelligence value. We believe that the quality of the estimate is limited by the mottle texture in the data, which would not be present with field data. By analyzing the smallest feature in the estimated silhouette, the helicopter refueling probe, we determined that the resolution achieved on the slide was 35μm which traces to 35cm resolution on a geosynchronous satellite. This corresponds to collecting data with a 60m linear array of 100 hobby telescopes, each 30cm in diameter and separated by 60cm (50% duty cycle). This resolution could also have been achieved by conventional imaging of an illuminated silhouette in GEO using a 60m-diameter telescope in the absence of any turbulence-induced or instrumental aberrations! The simulation of such a diffraction-limited image is shown in Fig. 5(c) for reference. This is a much larger diameter than any current telescope and the corresponding SASI system would be far easier to design and construct.

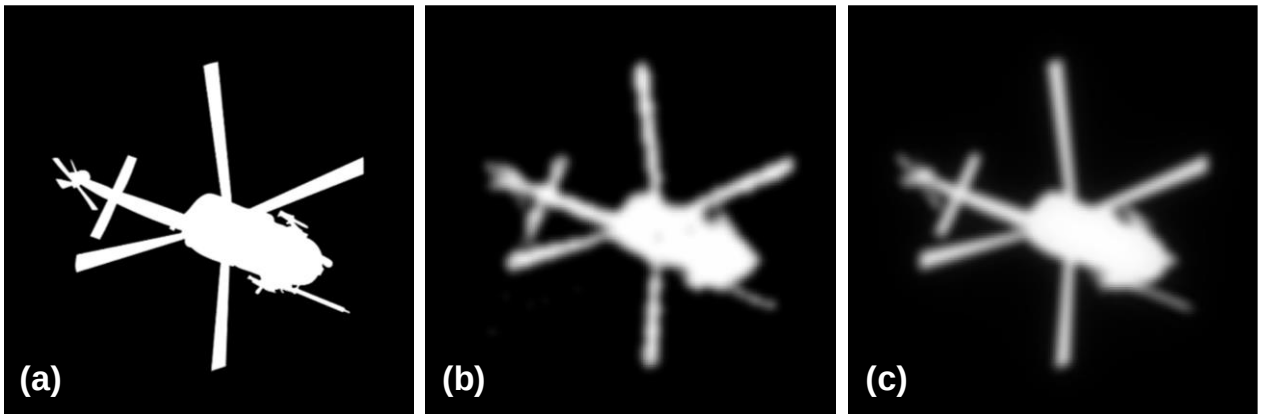

Fig. 5. Comparison of SASI restoration with reference images. (a) True silhouette design, as used for chrome deposition on the microscope slide. (b) Result of SASI restoration, using data shown in Fig. 4(a). Simulated diffraction-limited image that would be obtained from a 60m-diameter telescope in the absence of atmospheric turbulence.

5. CONCLUSIONS AND FUTURE WORK

We have designed and executed a SASI laboratory-demonstration experiment which is traceable to the geometry of ground-based imaging of GEO satellites. Non-literal SASI data were collected and processed to get a fine-resolution literal silhouette of the target. We believe that the resolution performance was limited by a mottle texture observed in the data that derives from microscope-slide-induced phase aberrations. Such aberrations are artificial since no aberrations will be induced in the neighborhood of the satellite when collecting field data. The only phase aberrations that occur in field data are induced by atmospheric turbulence induced in the final 0.005% of the propagation path from GEO satellite to the detector plane. SASI data are immune to such phase aberrations since we are collecting only intensity data.

Despite the residual texture in the laboratory data, we were able to achieve 35μm resolution on the microscope slide, which scales to 35cm on a GEO satellite. This is the same resolution that would be achieved with conventional imaging

of a binary geosynchronous object using a 60m diameter telescope on the ground which has no optical or turbulence-induced aberrations. This is a much larger telescope than any current telescope and the AO correction for such a telescope would be extremely challenging. Furthermore, a SASI system will cost far less than a conventional system providing equivalent resolution. This laboratory demonstration, which traces to the GEO-satellite imaging geometry, illustrates the value of the SASI concept and provides credibility for previous simulation demonstrations.

Having demonstrated SASI in the laboratory, we next want to perform field demonstrations. Even collecting a wink-out trace with anticipated chirp-like fringes using a single telescope will be a significant milestone which will provide a confirmation of radiometric calculations. This can be followed by a coarse imaging demonstration with a small array of telescopes. Concurrent with these efforts, design trades can be performed in support of fielding an operational SASI observatory. It is important to design the hardware to maximize the detected signal. Nature provides almost 3 times as many stars for every unit increase in stellar magnitude (dimmer). Accordingly, SASI operational frequency is improved when we design a system that can operate on fainter stars. More signal can be collected by increasing the unit-telescope diameter, by including multiple spectral channels with the aid of a dispersive element and multiple APDs, and with various telescope-array designs.

SASI is a cued system. To function properly, the system needs to know roughly when an occlusion is going to occur so that all the telescopes can point to and track the star that will be occluded. We also need to know the satellite orbital parameters well enough to ensure that the "shadow track" on the ground intersects the linear array of telescopes. It has been shown that TLE data from the Space Surveillance Network is not sufficiently accurate to support a SASI data collect [8]. Instead, we will need to rely on more precise orbital determination technologies such as coherent Doppler ranging, laser ranging, and multi-static methods. Fortunately, there is a concerted effort to develop these technologies for use with GEO satellites and debris. Selection and adaptation of at least one of these technologies will be needed for cueing a SASI observatory.

6. ACKNOWELEDGEMENT, DISCLAIMER, AND DISTRIBUTION

This research was developed with funding from the Defense Advanced Research Projects Agency (DARPA). The views, opinions and/or findings expressed are those of the authors and should not be interpreted as representing the official views or policies of the Department of Defense or the U.S. Government. Approved for Public Release, Distribution Unlimited

7. REFERENCES

[1] R.H. Burns, V. Gamiz, J.J. Dolne, J. Lambert, and S. Long., "Shadow imaging of GEO satellites," *Proc. SPIE* **5896** (2005).

[2] J. Luu, L. Jiang, and B. Willard, "Shadow imaging efforts at MIT Lincoln Laboratory," in *Advanced Maui Optical and Space Surveillance Technologies Conference* (2008).

[3] D.M. Douglas, "Shadow Imaging of Geosynchronous Satellites," Ph.D. Dissertation, University of Arizona, Tucson (2014).

[4] D.M. Douglas, B.R. Hunt, and D.G. Sheppard, "Shadow imaging of geosynchronous satellites: simulation, image reconstruction, and shadow prediction," *Proc. SPIE* **9982** (2016).

[5] D.M. Douglas, B.R. Hunt, and D.G. Sheppard, "Shadow imaging of geosynchronous satellites," in *Advanced Maui Optical and Space Surveillance Technologies Conference* (2016).

[6] R.G. Paxman, "Synthetic-aperture silhouette imaging," in *Advanced Maui Optical and Space Surveillance Technologies Conference* (2016).

[7] D.M. Douglas, B.R. Hunt, and D.G. Sheppard, "Resolution limits for shadow imaging of geosynchronous satellites: analytic and simulated approaches," *Proc. SPIE* **10410** (2017).

[8] D.G. Sheppard, D.M. Douglass, and B.R. Hunt, "Recent developments in shadow imaging prediction," in *Advanced Maui Optical and Space Surveillance Technologies Conference* (2018).

[9] R.G. Paxman, K.W. Gleichman, A.S. Iacchetta, and B.M. Jost, "Synthetic Aperture Silhouette Imaging (SASI): Laboratory Demonstration" in *Computational Optical Sensing and Imaging*, OSA Topical Meeting (2020).

[10] R.G. Paxman, "Superresolution with an opacity constraint," in *Signal Recovery and Synthesis III*, Technical Digest Series 15 (Optical Society of America, Washington DC, 1989).

[11] R.G. Paxman, J.R. Fienup, M.F. Reiley, and B.J. Thelen, "Phase Retrieval with an Opacity Constraint in LAser IMaging (PROCLAIM)," in *Signal Recovery and Synthesis*, 1998 Technical Digest Series 11, 34-36 (Optical Society of America, Washington DC, 1998).

[12] J.R. Fienup, R.G. Paxman, M.F. Reiley, and B.J. Thelen, "3-D imaging correlography and coherent image reconstruction," in *Digital Image Recovery and Synthesis IV*, T.J. Schulz and P.S. Idell, eds., *Proc. SPIE* **3815-07** (1999).

[13] S.T. Thurman, R.T. DeRosa, and J.R. Fienup, "Amplitude metrics for field retrieval with hard-edged and uniformly illuminated apertures," *JOSA A* **26** (2009).

[14] J.W. Goodman, *Introduction to Fourier Optics*, Roberts and Company Publishers, 2005.